PNAS RESEARCH ARTICLE | CELL BIOLOGY
BIOPHYSICS AND COMPUTATIONAL BIOLOGY

Nuclear compression regulates YAP spatiotemporal fluctuations in living cells

Newsha Koushki[a,1], Ajinkya Ghagre[a,1], Luv Kishore Srivastava[a], Clayton Molter[a], and Allen J. Ehrlicher[a,b,c,d,e,f,2]

Edited by David Weitz, Harvard University, Cambridge, MA; received January 31, 2023; accepted June 4, 2023

Yes-associated protein (YAP) is a key mechanotransduction protein in diverse physiological and pathological processes; however, a ubiquitous YAP activity regulatory mechanism in living cells has remained elusive. Here, we show that YAP nuclear translocation is highly dynamic during cell movement and is driven by nuclear compression arising from cell contractile work. We resolve the mechanistic role of cytoskeletal contractility in nuclear compression by manipulation of nuclear mechanics. Disrupting the linker of nucleoskeleton and cytoskeleton complex reduces nuclear compression for a given contractility and correspondingly decreases YAP localization. Conversely, decreasing nuclear stiffness via silencing of lamin A/C increases nuclear compression and YAP nuclear localization. Finally, using osmotic pressure, we demonstrated that nuclear compression even without active myosin or filamentous actin regulates YAP localization. The relationship between nuclear compression and YAP localization captures a universal mechanism for YAP regulation with broad implications in health and biology.

YAP | Nucleus | mechanotransduction | cell mechanics | biophysics

Significance

Understanding the mechanoregulation of YAP activity is an essential step in characterizing diverse physiological and pathological processes, as well as engineering responses such as in stem cell differentiation. Here, we suggest that previously reported diverse mechanical YAP stimuli such as substrate stiffness, cell contractility, cell geometry, nuclear stiffness, LINC complex connectivity, and cell volume may be collectively united under the umbrella mechanism of asymmetric nuclear deformation. YAP activity scaling directly with nuclear deformation presents a well-prescribed biophysical target for biomedical and life science research.

Cells are not purely biochemical entities but are also subjected to physical stimuli and constraints in forces and mechanics (1). Correct recognition of and responses to mechanical cues are key to health, whereas dysfunctional responses are symptomatic and perhaps causative to numerous pathologies (2). Many mechanosensory mechanisms regulate transcription factors, which in turn dictate fundamental aspects of cellular function, homeostasis, and tumorigenesis (3–6). Yes-associated protein (YAP) is a crucial nucleocytoplasmic shuttling transcriptional coactivator that connects cellular mechanics and signaling cascades underlying gene expression, cell proliferation, and differentiation (5, 7–10). YAP protein is a key mechanosensory protein that becomes transcriptionally active when imported into the nucleus (5, 8, 11, 12). Aberrant YAP nuclear localization can cause dysfunction associated with multiple diseases, including fibrosis and diverse cancers as a result of uncontrollable cell proliferation and activating genes associated with oncogenic transcription factors (13–16). Since the spatiotemporal localization of YAP regulates critical cellular physiology and pathology in diverse contexts, understanding the mechanical stimuli that modulate YAP activity is a central goal of current cellular biology.

In addition to canonical Hippo pathway regulation via LATS 1 and 2 (8, 11) and Akt-mediated YAP phosphorylation (17–19), YAP is widely reported to be influenced by physical stimuli, such as microenvironment mechanics, with several studies suggesting that YAP nuclear localization and activity tends to increase with increasing substrate stiffness (5, 20, 21). This has led to the hypothesis that substrate stiffness directly influences YAP localization and downstream effects such as proliferation and differentiation through mechanotransduction (5, 22–24). However, the abrogation of these effects by cytoskeletal disruption demonstrates that YAP activity is not directly linked to substrate mechanics but rather driven by cytoskeletal processes such as actomyosin contractility which can be biased by substrate stiffness (5, 20, 25, 26). Contractility impacts diverse mechanosensors in the cell (27, 28), including the nucleus (4, 29). Additionally, stresses external to the cell directly applied to the nucleus trigger YAP localization (30), placing nuclear mechanics and deformation at the center of YAP mechanotransduction (31, 32).

Nuclear mechanics are largely determined by a family of intermediate filaments known as lamins, with lamins A and C (lamA/C) supporting the nucleus and modulating its elasticity (33–36). LamA/C expression levels also modulate nuclear rigidity; suppression of lamA/C softens nuclei and increases nuclear deformability (36–38), whereas lamA/C overexpression increases nuclear stiffness (38, 39). This influence of nuclear stiffness is critical as the same applied force results in dramatically different nuclei deformations. These biophysical changes may have a direct pathological impact; mutations in lamA/C are associated with impaired nuclear mechanotransduction, resulting in a variety of human diseases, including Emery–Dreifuss muscular dystrophy, Hutchinson–Gilford progeria syndrome,

Author affiliations: [a]Department of Bioengineering, McGill University, Montreal, QC H3A 0E9, Canada; [b]Department of Anatomy and Cell Biology, McGill University, Montreal, QC H3A 0C7, Canada; [c]Department of Biomedical Engineering, McGill University, Montreal, QC H3A 2B4, Canada; [d]Department of Mechanical Engineering, McGill University, Montreal, QC H3A 0C3, Canada; [e]Centre for Structural Biology, McGill University, Montreal, QC H3G 0B1, Canada; and [f]Rosalind and Morris Goodman Cancer Institute, McGill University, Montreal, QC H3A 1A3, Canada

Author contributions: A.J.E. designed research; N.K., A.G., and L.K.S. performed research; A.J.E. contributed new reagents/analytic tools; N.K., A.G., L.K.S., and C.M. analyzed data; and N.K., A.G., L.K.S., C.M., and A.J.E. wrote the paper.

The authors declare no competing interest.

This article is a PNAS Direct Submission.

[1]N.K. and A.G. contributed equally to this work.

[2]To whom correspondence may be addressed. Email: allen.ehrlicher@mcgill.ca.

This article contains supporting information online at https://www.pnas.org/lookup/suppl/doi:10.1073/pnas.2301285120/-/DCSupplemental.

Published July 3, 2023.

and cancer metastasis (36, 40–44). Physiologically, nuclear deformations are regulated by actomyosin contractility and its direct connections to the nucleus via the linker of nucleoskeleton and cytoskeleton (LINC) complex. Thus, understanding at a fundamental level how actomyosin contractility, nuclear stiffness, and nuclear deformation change YAP mechanotransduction in living cells would address complex challenges ranging from stem-cell engineering to cancer progression and cellular aging disorders, making it a timely, fundamental challenge in human health.

Although previous studies have predominantly focused on the role of traction stress, substrate stiffness, cell spread area, and nuclear flattening on YAP localization (5, 7, 20, 26, 30, 45, 46), the inherent coupling of these reported regulatory parameters (21, 47–49) has limited our understanding of the main and actual regulator of YAP and failed to clarify YAP dynamics in response to transient mechanical stimuli. Franklin et al. have recently reported fast oscillations of YAP nucleocytoplasmic localization (46), revealing that YAP localization is far from static in living cells. Nevertheless, the mechanism tuning YAP fluctuations in motile living cells remains unknown and is the key in unlocking dynamic YAP mechanotransduction. Previously, simulation work has suggested that nuclear deformation may be a central uniting mechanosensory (50); in this study, we provide direct and comprehensive evidence supporting this prediction. We track dynamic YAP localization in living cells and show that nuclear compression uniquely determines YAP localization in all explored experimental conditions. We resolve spatial and temporal correlated changes in both cell contractility and YAP distribution during cell movement on diverse substrate stiffnesses, suggesting that substrate rigidity alone does not proscribe YAP localization. Further, we show that mechanical work from cell contractility (strain energy) rather than cell traction stress induces YAP nuclear translocation through nuclear compression and does so independently of substrate stiffness. Decreasing nuclear stiffness via siRNA of lamA/C dramatically increases cell contractility–induced nuclear compression and YAP activation, demonstrating that the effective nuclear deformation rather than applied contractility regulates YAP localization. We further demonstrate that mechanical work from extracellular sources that also compress the nucleus induces the same YAP localization, even in the absence of an actin cytoskeleton. These findings reveal that it is the resultant nuclear compression, and not the applied stress, nuclear stiffness, or microenvironment mechanics, which regulates YAP localization.

Results

YAP Localization Is Highly Dynamic in Spread Living Cells Regardless of Substrate Elasticity. To examine the YAP localization in living cells, we transfected NIH 3T3 cells with enhanced green fluorescent protein (EGFP)-YAP (pEGFP-C3-hYAP1, a gift from Marius Sudol, Addgene, plasmid #17843) and with EBFP2-Nucleus-7 (nuclear localization signal, Addgene, plasmid #55249) to visualize the nucleus. Similar to previous studies, our principal metric for YAP quantification is the ratio of fluorescence of EGFP-YAP in the nucleus to EGFP-YAP in the cytoplasm and is henceforth referred to as the YAP Ratio (YR), where total endogenous and EGFP-YAP appear similarly distributed in the cell (*SI Appendix*, Fig. S1). We first compared the YRs of endogenous YAP and exogenous EGFP-YAP as cells spread on polydimethylsiloxane (PDMS) substrates (51, 52) with different Young's moduli (0.3 and 48 kPa). Critically, these silicone substrates are linearly purely elastic as demonstrated previously (51, 52), in contrast to commonly employed strategies of diluted crosslinking that result in incompletely percolated viscoelastic PDMS substrates (53, 54). Using these elastic substrates, we quantified YRs on soft PDMS, stiff PDMS, and very stiff glass substrates in both transfected and immunostained cells (Fig. 1 *A*–*C* and *SI Appendix*, Fig. S2). Here, we found no significant trends in EGFP or endogenous YR between soft PDMS and stiff glass.

When we examined EGFP-YAP fluctuations during cell movement on PDMS substrates, we observed that EGFP-YAP localization is highly dynamic in time, yet has no visible correlation with substrate stiffness across diverse PDMS substrate moduli (0.3, 2, 5, 12, 18, and 100 kPa) as well as fibronectin-coated glass (Fig. 1 *D*–*F* and *SI Appendix*, Figs. S2 and S3). The time-averaged YR and YR distributions on stiff substrates appeared identical to compliant substrates, demonstrating that neither the magnitude of YAP localization nor the shuttling frequency appears set by PDMS substrate stiffness in high spread area cells (Fig. 1 *D*–*F*). These results contrast with previous reports of cytoplasmic enrichment of YAP on soft polyacrylamide (PAA) substrates and a general positive correlation between the YR and substrate stiffnesses (5, 20, 30). Nevertheless, a recent study has shown that while average YR does tend to increase with substrate stiffness, that YR is highly dynamic and displays a broad distribution on all PAA substrate moduli, with the broadest distribution on the softest substrate (0.4 kPa) (46).

To examine the impact of substrate material selection (PDMS or PAA) on EGFP-YAP localization, we prepared PAA gels with uniform polymer mass and tuned the stiffness by varying the bis crosslinker concentration. Cells on very compliant PAA substrates with Young's modulus of 1 kPa were round and sessile, with small spread areas and more cytoplasmic sequestration of YAP (YR < 1), consistent with previous findings (Fig. 1 *G* and *H* and *SI Appendix*, Fig. S2). Cells seeded on very compliant PDMS substrates (0.3 kPa) displayed a wide range of spread areas and oscillations in YAP localization, similar to those cells on the stiff PDMS and PAA substrates (Fig. 1 *D*–*H* and *SI Appendix*, Fig. S2). These results are also consistent with the previous report of dynamic YAP in motile spread cells (46), suggesting that our observed PAA very soft substrate sensitivity is limited due to a lack of cell spreading and adhesion; in active cells with more spreading, however, YAP is dynamically distributed between the nucleus and cytoplasm in all of our PDMS measurements, which are quantitatively consistent with published dynamics of YR on mechanically diverse PAA substrates (46).

To examine more closely the roles of substrate adhesion and cell spread area on YAP translocation, we also tracked YAP localization in suspended cells during their attachment (Fig. 1*I*). Before initial cell attachment, we measured consistent cytoplasmic YAP (low YRs) in round cells with a small projected area (<~1,200 μm^2) (Fig. 1*I*). After adhering and spreading, however, YAP fluctuated between the nucleus and cytoplasm with no clear trend with cell area (Fig. 1*I*).

These results and previous findings highlight that while substrate stiffness does appear to bias YR in cells, the variance of YR observed across all substrates shows that substrate stiffness does not precisely proscribe YAP activity, suggesting another mechanism in play. Indeed, all known prior works investigating the role of substrate stiffness have reported that cytoskeletal disruption inhibits any measured substrate-dependent YAP localization (20, 30, 55). This demonstrates that substrate stiffness may bias intracellular cytoskeletal processes; however, these cytoskeletal responses more directly regulate YAP localization. We thus suspected that dynamic changes in cytoskeletal cell contractility, as may be induced by different substrate moduli, lead to dynamic and correlated changes in YAP localization.

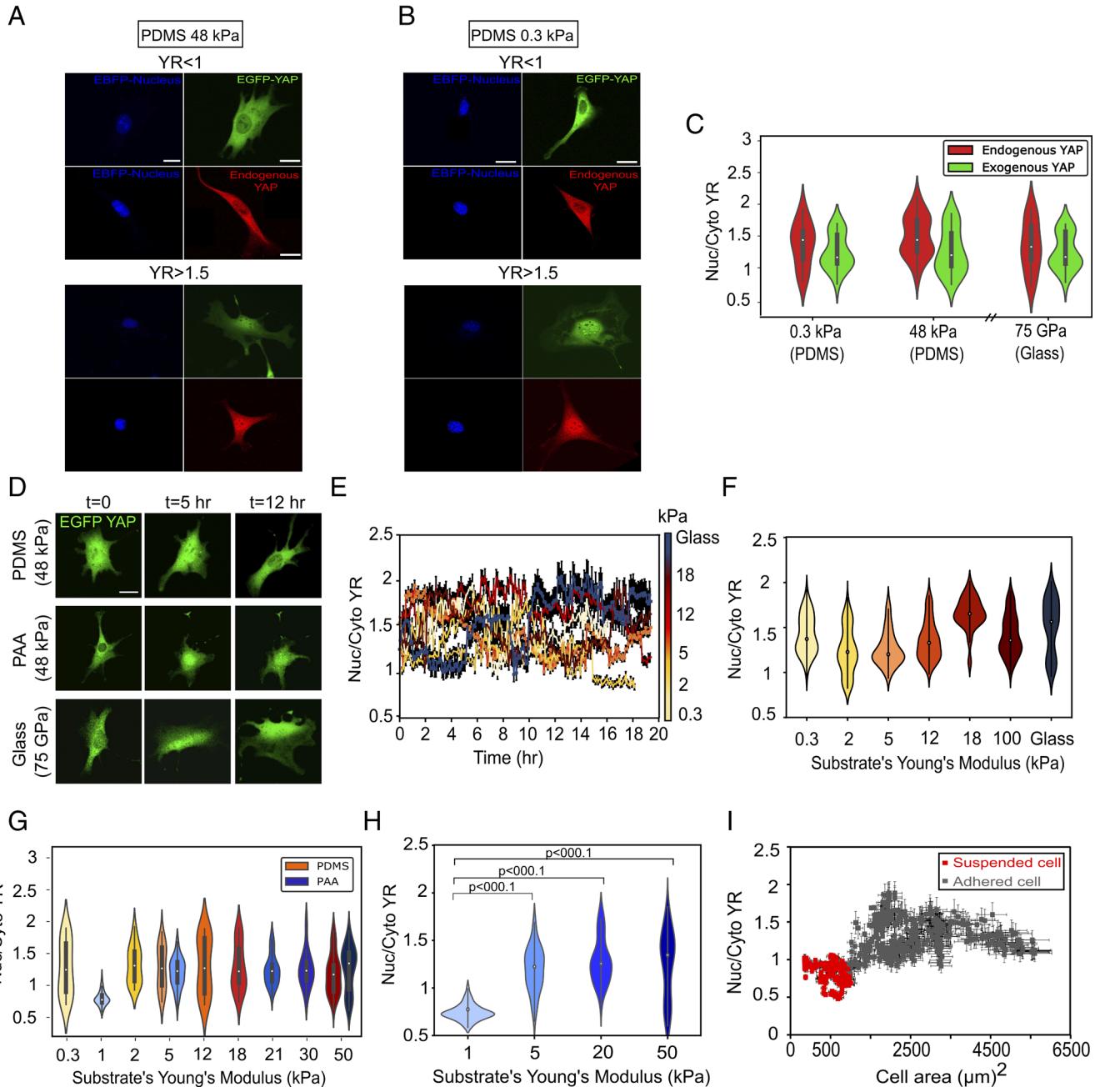

Fig. 1. YAP localization is highly dynamic in spread living cells on substrates with diverse elastic moduli. (*A*) Example images of EGFP-YAP and endogenous YAP merged with the EBFP-NLS nucleus on stiff PDMS and (*B*) soft PDMS. (*C*) Violin plots of YR variations on soft, stiff PDMS, and glass for EGFP transfected and endogenous YAP (n = 40 single cells per each condition). (*D*) Examples of EGFP-YAP variation during cell movement on PDMS, PAA, and glass over time. (*E*) Time course of EGFP-YAP YR during cell movement on PDMS substrates with various stiffnesses and on the fibronectin-coated glass. (*F*) Time-averaged EGFP-YAP YR and violin plot of YR in the same condition as in (*E*). (*G*) EGFP-YAP YR variations on PDMS (shades of red) and PAA (shades of blue) substrates with different stiffnesses (n = 35 cells per each condition). (*H*) Violin plots of EGFP-YAP YR variations in transfected cells moving on PAA substrates with diverse stiffnesses, *P* values obtained from the pairwise *t* test, and values below 0.0001 suggest a statistically significant difference. (*I*) Quantification of EGFP-YAP YR and cell area before (red) and during cell attachment (gray) on 5 kPa PDMS (n = 17 cells). Scales bars are 20 μm for the cells and 10 μm for the nuclei. Error bars indicate SD.

Cell Strain Energy Regulates YAP Nucleocytoplasmic Shuttling Independent of Substrate Elasticity. We employed traction force microscopy (TFM) (56, 57) to track single-cell contractility (traction stress and strain energy) in time on PDMS substrates with different Young's moduli (0.3 and 5 kPa) (51, 52) and compared these metrics with dynamic YRs. The strain energy is the total contractile work generated by the cell. This is different from RMST which is the rms (average) traction stress that cells apply to the substrate (*Materials and Methods*).

We found that on all substrates, the contractile state of the motile spread cell changed in time, and the cell contractility was temporally correlated with the YR (Fig. 2 *A*–*E* and *SI Appendix*, Fig. S3). These results explain YAP's dynamic movement during cell migration on each substrate. We then compared the time-varying contractile states of single cells with their YRs over a broad range of substrate stiffnesses, finding that both cell traction stress and the underlying average cell-induced substrate deformation as reported by fiduciary bead displacement were correlated with YRs for individual cells (Fig. 2 *F*

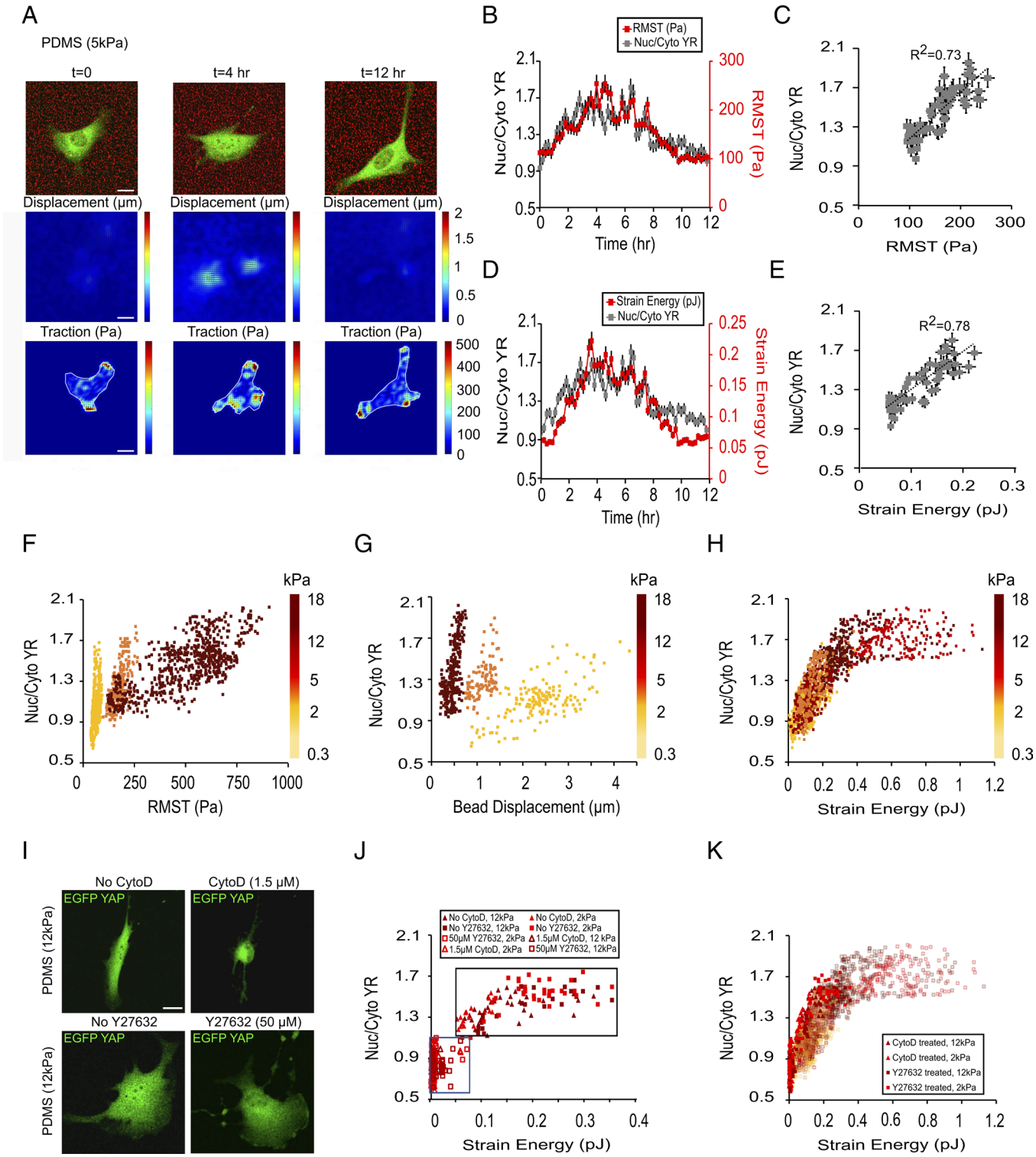

Fig. 2. Cell strain energy regulates YAP nucleo-cytoplasmic shuttling independent of substrate elasticity. (*A*) Representative images, local bead displacement, and traction stress maps of EGFP-YAP transfected NIH 3T3 cell during its movement on 5 kPa PDMS substrate. (*B*) Time course of EGFP-YAP YR and RMST for the same cell as in (*A*) (duration: 12 h, time interval: 12 min). (*C*) EGFP-YAP YR as a function of RMST for the same condition as in (*A*) and (*B*). (*D*) Quantification of EGFP-YAP YR and strain energy for the same cell over time. (*E*) EGFP-YAP YR vs. strain energy for the same cell, (*F*) EGFP-YAP YR vs. average RMST for multiple cells seeded on PDMS substrates with different stiffnesses [n = 146 cells for PDMS 0.3kPa (yellow), n = 135 cells for PDMS 2kPa (orange), and n = 278 cells for PDMS 18kPa (brown)], (*G*) EGFP-YAP YR vs. average bead displacement for the same cells as in (*F*). (*H*) YR as a function of strain energy for the cells in (*F*) (data related to the cells seeded on 5 and 12 kPa were added). (*I*) Example of EGFP-YAP transfected cells before and after pharmacological treatments. (*J*) Quantification of EGFP-YAP YR vs. strain energy for multiple cells on PDMS substrates with different Young's moduli before (solid markers) and after (open markers) pharmacological treatments (n = 68 cells for Y27632 treatment, and, n = 57 cells for CytoD treatment). (*K*) All data of EGFP-YAP YR as a function of strain energy for nontreated (partially transparent open square data) and pharmacologically treated cells (solid data). Scale bars are 20 μm. Error bars indicate measurement error.

and *G*). Thus, while substrate stiffness alone did not appear to regulate YR during cell movement, cell traction stress and substrate displacement were shown to impact YAP localization. YRs were correlated with contractile stress yet separated into different populations as a function of substrate stiffness (Fig. 2 *F* and *G*). These results reveal that on both soft and stiff PDMS substrates, YAP can localize

to the cytoplasm or nucleus depending on the contractile stress of the cell corresponding to that substrate stiffness; spread cells on soft PDMS were shown to trigger YAP nuclear localization (YR > 1.5) with lower traction stress than those seeded on stiff PDMS. We then examined the effects of cell strain energy (contractile work) which previously was shown to be independent of substrate stiffness (57) on YAP activity. We found that the dependence of YR on cell contractile work was independent of substrate stiffness with all data from different substrate rigidities collapsing onto a single curve, suggesting that cell contractile work describes YAP localization in diverse microenvironment mechanics (Fig. 2*H*).

To quantify how changes in contractility would influence YAP localization, we then disrupted myosin activity and the actin cytoskeleton by adding ROCK inhibitor (Y-27632) and cytochalasin D (CytoD), respectively (*Materials and Methods*). Both pharmacological treatments inhibited cell contractility and concordantly suppressed YAP nuclear localization ~15 and ~40 min after adding CytoD and ROCK inhibitor, respectively (Fig. 2 *I* and *J* and *SI Appendix*, Fig. S3). Critically, these cytoskeletal disruptions did not change the relationship between cell contractility and YR, and data from cytoskeleton-disrupted cells all followed the same YAP localization–strain energy curve, where weaker contractility leads to reduced YRs (Fig. 2*K*). These results demonstrate that contractile work is a better predictor of YAP localization than traction stress during cell movement on different substrates and across all probed cytoskeletal states.

As contractile work appears to determine YAP localization across a broad range of conditions, we considered the cellular components that are mechanically impacted by cell contractile work and may drive changes in the YR. Since the nucleus is the locus of YAP activity and has been implicated in force-mediated YAP localization (4, 30, 55, 58), we examined how contractile work mechanically compresses the nucleus and relates to YAP nuclear localization.

Cell Strain Energy Modulated Nuclear Volume Is a Unique Determinant of YAP Localization. To examine the interplay between cell work and nuclear deformation, we quantified the nuclear volume using confocal Z-stacks for cells with different contractility. Examining different cellular contractile states, we found decreased nuclear volume for cells with higher contractile work, leading to an inverse relationship between nuclear volume and cell strain energy (Fig. 3 *A* and *B* and *SI Appendix*, Fig. S4). Traction stress, however, showed a weak correlation with nuclear volume on different substrate stiffnesses, suggesting that cell strain energy has a more critical role in force transmission to the nucleus corresponding to the nuclear compression (*SI Appendix*, Fig. S4). We then considered the mechanical connection which facilitates contractile work to compress the nucleus. One key component between actomyosin contractile machinery and the nuclear envelope is the LINC complex (4, 30, 34). When we disrupted the LINC complex via dominant-negative GFP-Nesprin1-Klarsicht, ANC-1, Syne Homology (KASH) and GFP-Nesprin2-KASH (DNK1/2) plasmids (*Materials and Methods* and *SI Appendix*, Fig. S5), we

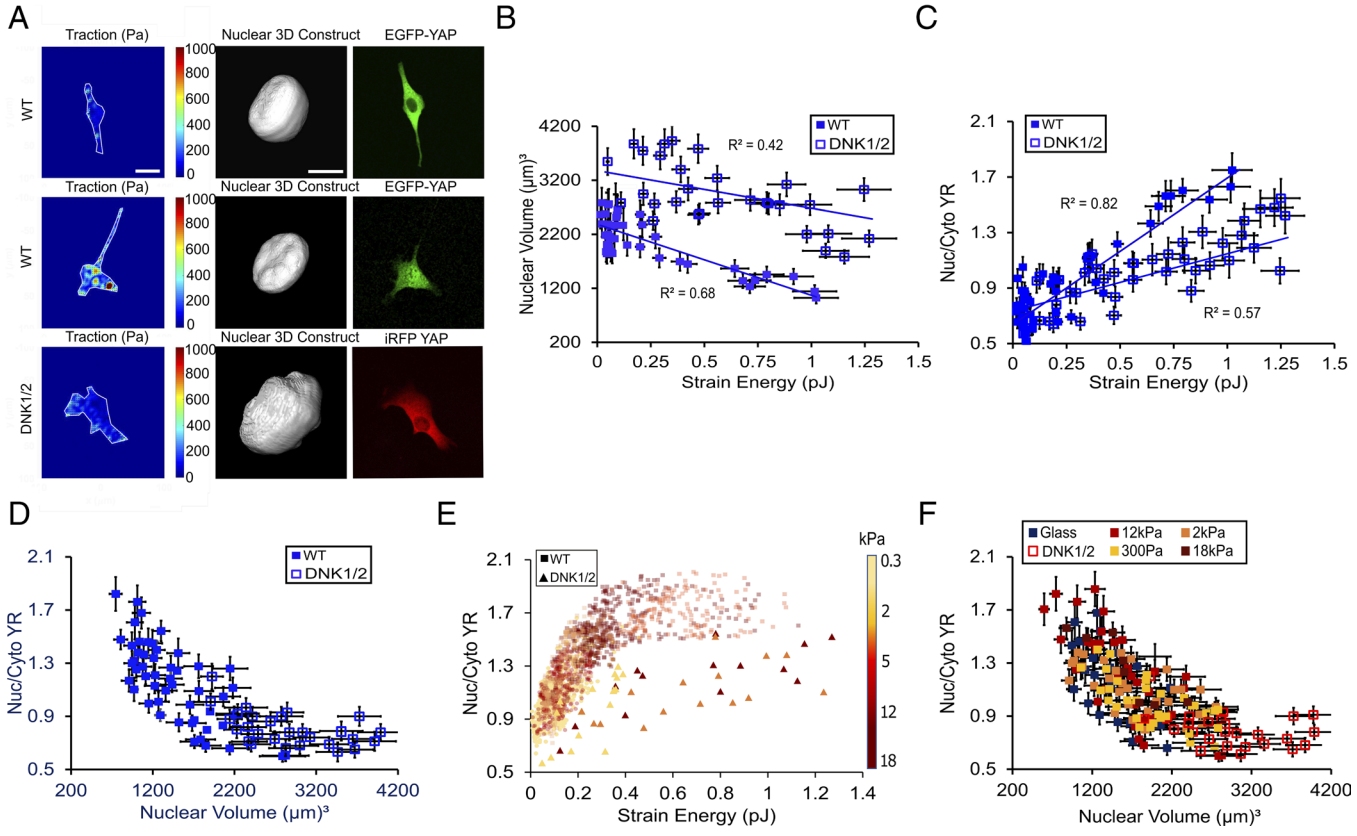

Fig. 3. Cell strain energy modulated nuclear volume is a unique determinant of YAP localization. (*A*) Representative traction stress maps, nuclear volumes, and EGFP-YAP distributions in WT and DNK1/2 overexpressed (LINC disrupted) cells with diverse contractility states on 12 kPa PDMS. (*B*) Quantification of nuclear volume vs. strain energy for WT and DNK1/2 cells on 12 kPa PDMS (n = 35 WT cells and n = 28 DNK1/2 cells). (*C*) Quantification of EGFP-YAP YR vs. strain energy for the same cells as in (*B*). (*D*) YR as a function of nuclear volume for the same cells as in (*B*). (*E*) EGFP-YAP YR vs. strain energy in WT (squares) and DNK1/2 (triangles) cells seeded on PDMS substrates with different stiffnesses. The color bar is representative of substrate stiffness (n = 15 DNK1/2 cells per each PDMS stiffness). (*F*) Relationship between EGFP-YAP YR and nuclear volume for DNK1/2 and WT cells seeded on different PDMS substrates (n = 25 DNK1/2 cells, n = 33 WT on PDMS 0.3 kPa, n = 28 WT on 2 kPa, n = 30 WT on 12 kPa, n = 17 WT on 18 kPa, and n = 27 WT on glass). Scale bars are 20 μm for cells and 10 μm for nuclei. Error bars indicate measurement error.

found that nuclear volumes were generally larger relative to wild-type (WT) cells for any given cell contractility, demonstrating less efficient mechanical coupling between the nucleus and cytoskeletal contraction (Fig. 3 *A* and *B*). Paralleling this observation, disrupting the LINC complex also reduced YRs for any given cell contractile work (Fig. 3 *C* and *E* and *SI Appendix*, Fig. S4). This suggests that contractile work (as measured by TFM) is not a unique determinant of YAP localization, but rather how contractility impacts the nucleus is critical. Quantifying the relationship between YRs and nuclear volume for cells cultured on 12 kPa PDMS, we found a complete overlap between both WT and LINC complex disrupted data, suggesting that nuclear volume in both cases directly regulates YRs (Fig. 3*D*). Our results also demonstrated that cell contractility-driven nuclear compression is correlated with YAP nuclear localization independent of substrate stiffness (Fig. 3*F*), with no trend between nuclear volumes and substrate stiffnesses (*SI Appendix*, Fig. S4) and similar YR and nuclear volume trends in both WT and LINC disrupted cells (Fig. 3*F*). These findings illustrate that the nuclear volume is a more robust physical parameter than cell contractility regulating YAP independent of cytoskeletal state and microenvironment (Fig. 3*F*).

We then questioned how mechanisms which impact nuclear deformation, such as varying nuclear stiffness, would impact YAP localization by modulating the amount of deformation for a given cell contractility. Prior work has demonstrated that modulating lamA/C expression significantly impacts nuclear stiffness (59, 60). This suggested to us that changes in lamA/C expression would result in changes in nuclear deformation for a given contractile work and lead to changes in YAP mechanotransduction.

LamA/C Suppression Facilitates YAP Nuclear Translocation via Increasing Nuclear Deformability. Exploiting the role of lamA/C in nuclear stiffness (59–61), we suppressed lamA/C expression using doxycycline-dependent inducible shRNA (*Materials and Methods* and *SI Appendix*, Fig. S6). To quantify total single-cell lamA/C expression levels, we transfected the cells with GFP-lamA/C chromobody which labels all the lamA/C inside the nucleus, allowing us to measure nuclear stiffness as a function of lamA/C expression (Fig. 4 *A* and *B*) (62). We measured corresponding nuclei compression under varied osmotic stresses applied by different concentrations of 400 Da polyethylene glycol (PEG) (*SI Appendix*, Fig. S4). From the corresponding applied stresses and measured nuclear volumetric compression, we determined the nuclear stiffness (*Materials and Methods*) (Fig. 4*B*) (63). We measured softer nuclei with higher nuclear deformability (lower bulk modulus) in lamA/C silenced cells compared to WT cells, consistent with previous findings (Fig. 4*B* and *SI Appendix*, Fig. S4) (59–61).

We then examined how contractile work compresses nuclei with different stiffnesses, and how this in turn regulates YAP localization. Interestingly, lamA/C silenced cells (with more compliant nuclei) (Fig. 4*B*) had smaller nuclei across a range of contractile work with volumes that were more sensitive to changes in contractility, leading to increased YRs at low contractility (Fig. 4*C*). In comparison, WT nuclei were relatively larger, requiring more contractile work to compress them and localize YAP therein (Fig. 4 *C* and *D*). Examining the relationship of nuclear volume on YAP distribution, we found that YAP ratio was correlated with the nuclear volume across diverse lamA/C expression levels in WT

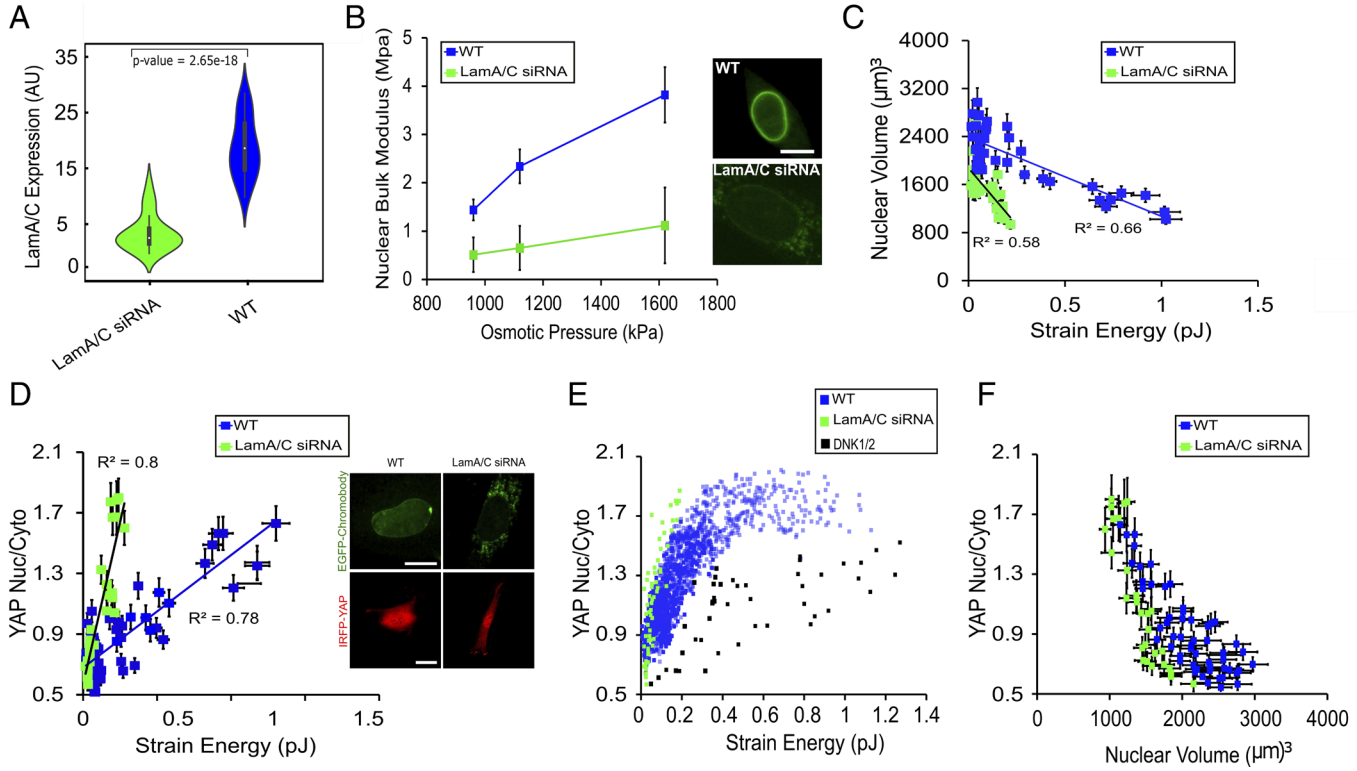

Fig. 4. LamA/C suppression facilitates YAP nuclear translocation via increasing nuclear deformability. (*A*) Violin plot of lamA/C expression level for lamA/C siRNA and WT cells (n = 29 lamA/C siRNA; n = 33 WT cells). *P* values obtained from the pairwise *t* test, and values below 0.0001 suggest a statistically significant difference. (*B*) Quantification of nuclear bulk moduli under different osmotic pressures applied to lamA/C siRNA and WT cells (n = 35 cells per each condition). The *Inset* image is an example of lamA/C expressions in GFP-lamA/C chromobody transfected WT and lamA/C silenced cells. (*C*) Quantification of nuclear volume vs. strain energy for cells with different lamA/C expression levels (n = 31 WT and 28 lamA/C siRNA cells). (*D*) EGFP-YAP YR vs. strain energy for the same cells as in (*C*). The *Inset* image exemplifies GFP-Chromobody and iRFP-YAP in WT and lamA/C silenced cells. (*E*) All data of EGFP-YAP YR as a function of strain energy for WT (blue markers), lamA/C siRNA (green markers), and DNK1/2 cells (black markers) (n = 48 DNK1/2 and n = 63 lamA/C siRNA cells). (*F*) YR vs. nuclear volume for the same condition as in (*C*). Scale bars are 20 μm for cells and 10 μm for nuclei. Error bars in panel *B* indicate SD and in other panels measurement error.

and lamA/C silenced cells (Fig. 4*F*). Consistent with our LINC studies, this demonstrates that nuclear compression and YR are not uniquely proscribed by contractile work (Fig. 4 *C*–*E*), but rather by the ensuing nuclear compression (Fig. 4*F*). In addition to lamA/C, chromatin condensation is also known to regulate nuclear mechanics (64); to test whether nuclear softening via chromatin mechanics has a similar effect on nuclear compression and YR, we employed the drug SAHA to decondense chromatin and soften the nucleus (65, 66). Here, we observed a SAHA dose-dependent decrease in nuclear volume along with an increase in YR, suggesting that nuclear softening in general does lead to higher contractility-driven nuclear compression and a complementary rise in YR (*SI Appendix*, Fig. S13). Having observed a correlation between YR and contractility-driven nuclear volume under the diverse conditions of cytoskeletal poisons, LINC suppression, and varied lamA/C expression, we postulated that modifying nuclear volume through any mechanism may be sufficient to induce YAP nuclear localization.

Nuclear Compression Alone Is Sufficient to Trigger YAP Nuclear Localization Independent of Contractile Work, Actin Filaments, LINC Complex, and Nuclear Stiffness. To test this hypothesis, we applied external osmotic stresses on the cells using different concentrations of PEG400 and measured nuclear volumes and YRs for cells under different osmotic pressures (*Materials and Methods*). We observed a significant increase in YAP nuclear localization under 10% PEG (1.62 MPa osmotic pressure), whereas 2% PEG (960 kPA) was not sufficient to trigger YAP nuclear entry (*SI Appendix*, Fig. S7), with similar changes in both endogenous and EGFP-YAP (*SI Appendix*, Fig. S8). Our results revealed the same conserved relationship between nuclear volume and YAP localization (Fig. 5 *A* and *B*). To ensure that EGFP-YAP accurately reports trends in the endogenous localization of YAP under osmotic pressure, we compared YAP ratios in separate experiments as measured by immunofluorescence and EGFP-YAP quantification. We examined the YR as functions of volume with and without osmotic compression, finding that both endogenous and EGFP-YAP nuclear localization trends both scale inversely with nuclear volume (*SI Appendix*, Fig. S12). To examine whether this relationship is unique to NIH 3T3 or displayed in other cells as well, we measured the nuclear volume and endogenous YAP ratio in immunostained human dermal fibroblasts before and after adding different concentrations of PEG. This revealed a quantitatively similar relationship, suggesting that it may be exploited by cell biology in general (*SI Appendix*, Fig. S9). To eliminate the possibility that this may be solely ascribed to an osmotic stress artifact, we also mechanically compressed cells using small, weighted agarose pads (*Materials and Methods*), revealing that mechanical vertical compression of cells also induces YAP nuclear localization (*SI Appendix*, Fig. S14).

Next, we examined the role of the actin cytoskeleton in adhered cells in osmotic pressure–mediated YAP activity by depolymerizing F-actin with Cytochalasin D (CytoD). After depolymerizing actin filaments, nuclear volumes increased and YRs decreased, illustrating a nuclear compressive role for actomyosin contractility (Fig. 5 *C* and *D*). After applying an osmotic pressure (5% PEG400, 1.12 MPa), we again observed increased YAP nuclear translocation with decreasing nuclear volume (Fig. 5 *C* and *D*). These results demonstrated that the actin cytoskeleton is not essential for YAP mechanotransduction. We also revisited the role of the LINC complex in YAP nuclear localization under external pressure by interrupting the LINC complex via overexpression of DNK1/2. Interestingly, compared to WT cells, a lower osmotic pressure (1.12 MPa) was required to substantially compress the nucleus and activate YAP in both CytoD and LINC disrupted cells (Fig. 5 *C*–*F*). These findings demonstrated that external forces compress the nucleus and localize YAP even in the absence of filamentous actin and the LINC complex. We also observed that the nuclei of LINC-disrupted and CytoD-treated cells compressed relatively more under the same amount of pressure as compared with WT cells, further suggesting a potential mechanoprotective role for LINC and the cytoskeleton in the context of external compression (*SI Appendix*, Fig. S7). Critically, all YAP activity and nuclear volume data for WT, CytoD-treated, and LINC-disrupted cells appear as a single correlated distribution across all experimental conditions demonstrating a robust connection between nuclear volume and YAP localization (Fig. 5*G*). These diverse data suggest a strong preserved correlation between nuclear volume and YR; however, we questioned whether changing nuclear volumes in a given set of cells would direct changes in YRs, demonstrating a causal role for nuclear compression in YAP localization. To examine this, we simultaneously quantified the changes in nuclear volume ($-\Delta V/V_0$) and in YAP ratios ($\Delta YR/YR_0$), while applying varying osmotic pressures to WT, LINC-disrupted, and CytoD-treated cells. For all examined conditions, the change in YR as a function of change in nuclear volume fell on a single curve, demonstrating that nuclear compression regulates YAP localization in a magnitude-dependent and conserved manner (Fig. 5*H*). To examine the time–response of YAP import, we also performed high-temporal resolution experiments, revealing an acute increase of YAP nuclear import within 1 s of compression, followed by a steady increase of YAP nuclear localization over approximately 10 min (*SI Appendix*, Fig. S10). To determine whether YAP import is regulated by applied stress of nuclear strain, we examined the role of nuclear softening induced by silencing lamA/C on osmotic stress–mediated YAP localization, finding that siRNA lamA/C cells required lower osmotic pressure (960 kPa) than WT cells (1.12 MPa) to compress nuclei and localize YAP in the nucleus (Fig. 5*I*), driven by both active and passive import processes (*SI Appendix*, Fig. S11). We also compared the effects of swelling via hypotonic media to compression via hypertonic media, finding that nuclear compression triggers YAP translocation, whereas nuclear swelling does not (*SI Appendix*, Fig. S15). These findings reveal nuclear compression as the dominant YAP mechanosensing mechanism and describe a preserved causal relationship between nuclear compression and YAP localization (Fig. 6).

Discussion

Diverse studies have examined how YAP activity is impacted by cell contractile stress (traction stress) in a substrate stiffness–dependent way; generally, it has been previously observed that cells on soft substrates have YAP mostly localized in the cytoplasm, whereas cells on stiff substrates mediate YAP nuclear translocation (5, 30, 67). However, in prior studies, substrate stiffness impacted YAP localization through varying cell morphology across different stiffnesses; soft substrates resulted in small round cells with cytoplasmic YAP localizations, while stiff substrates induced highly spread cells with predominantly YAP nuclear localizations (5, 20, 21, 30). In addition, previous studies reported YAP nuclear localization by applying external forces (30, 45, 68), such as stretching of the cells on soft substrates (45), suggesting that substrate stiffness alone is not an independent regulator of YAP activity. Indeed, prior work has demonstrated that beyond their stiffness, surface stresses of silicones can also increase stresses acting on cells, particularly at moduli below 2 kPa (69). This additional surface stress from silicones likely resolves discrepancies between PAA and PDMS on soft substrates observed here and previously (54, 70). While cell-generated forces

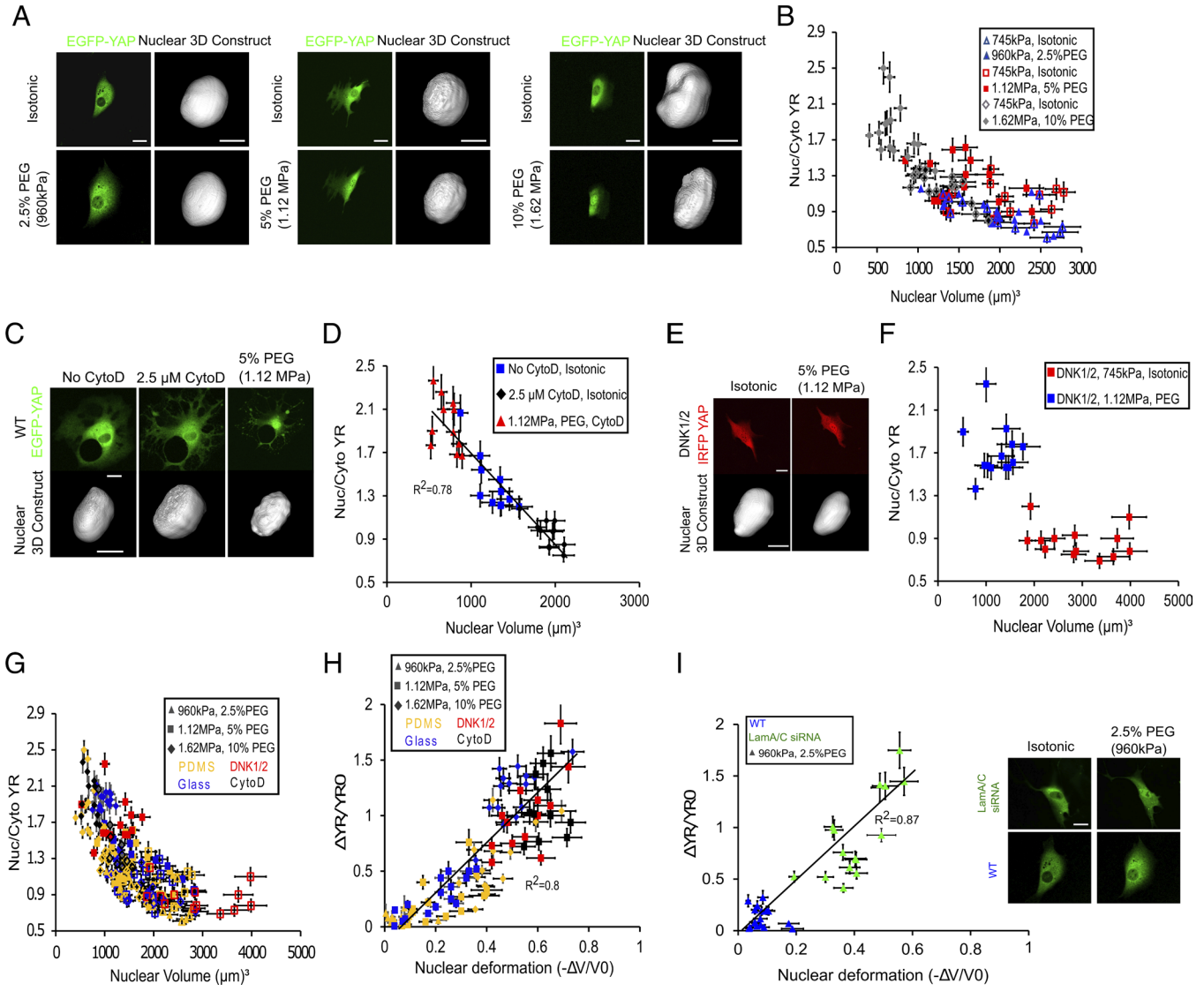

Fig. 5. Nuclear compression alone is sufficient to trigger YAP nuclear localization. (*A*) Examples of YAP localization and nuclear volume of the cells under different osmotic pressures. (*B*) Quantification of YR vs. nuclear volume in isotonic (open markers) and hyperosmotic conditions (solid markers) (n = 12 cells under 2%, n = 14 cells under 5%, and n = 15 cells under 10% PEG400). (*C*) Example of changes in nuclear volume and EGFP-YAP localization in CytoD treated cells after applying 5% PEG400 (1.12 MPa osmotic pressure). (*D*) Quantification of EGFP-YAP YR vs. nuclear volume in isotonic condition (blue squares), 30 min after adding 2.5 μM CytoD (black diamonds), and 20 min after adding 5% PEG400 (red triangle) (n = 10 cells). (*E*) Example of changes in iRFP-YAP localization and nuclear volume in GFP-DNK1/2 transfected cells before and after adding 5% PEG400. (*F*) Quantification of iRFP-YAP YR vs. nuclear volume for LINC disrupted cells before (red squares) and after (blue squares) adding 5% PEG400 (n = 13 cells). (*G*) All data of EGFP-YAP YR vs. nuclear volume for CytoD-treated (black markers), iRFP-YAP YR DNK1/2 (red markers) transfected cells seeded on the glass, and EGFP-YAP WT cells seeded on the glass (blue markers) and 300 Pa PDMS (yellow markers) under different hyperosmotic conditions. All open markers and solid markers are representative of isotonic and hyperosmotic conditions, respectively (n > 10 cells per each condition). (*H*) Quantification of normalized YR change as a function of nuclear volumetric compression for the same values measured in (*G*). (*I*) YR change vs. nuclear compression for WT and lamA/C siRNA cells before (open markers) and after applying 960 kPa osmotic pressure (solid markers) (n = 15 cells per each condition). The *Inset* image is an example of EGFP-YAP YAP localization in WT and lamA/C silenced cells under 2.5% PEG400. Scale bars are 20 μm for the cells and 10 μm for the nuclei. Error bars indicate measurement error.

on soft PAA may remain low, with the additional surface stresses from silicones, the total stresses (cell + surface) are sufficient to support cell spreading, increased forces, and resulting mechanobiology. This further highlights the importance of quantifying actual stresses at the cell–substrate interface, as with TFM, rather than considering substrate compliance alone. Nevertheless, even in the context of differential surface stresses, we see a conserved relationship between nuclear volume and YAP localization, further suggesting that stresses of any origin promote the observed nuclear volume mechanotransduction.

Our results illustrate that YAP is highly dynamic in living cells on all investigated substrate stiffnesses, and its localization is robustly defined by the nuclear compression induced by cell strain energy or extracellular forces, complementary to previous work investigating the role of "nuclear flattening" (i.e., vertical deformation) in YAP mechnaotransduction (30). Our study offers nuclear compression as a ubiquitous mechanical explanation of non-Hippo YAP regulation, accounting for previously identified diverse mechanical stimuli of YAP regulation, including substrate stiffness (5, 20, 21), cell contractility (20, 21, 30), and nuclear compression (4, 30, 55, 68). To resolve how these apparently separate mechanoregulatory mechanisms actually influence the same one of nuclear compression, we first examined cell contractility and YAP; this explained previously observed dynamic fluctuations in YAP localization (46, 71) to the variations in cell contractility during cell movement on a specific substrate. We

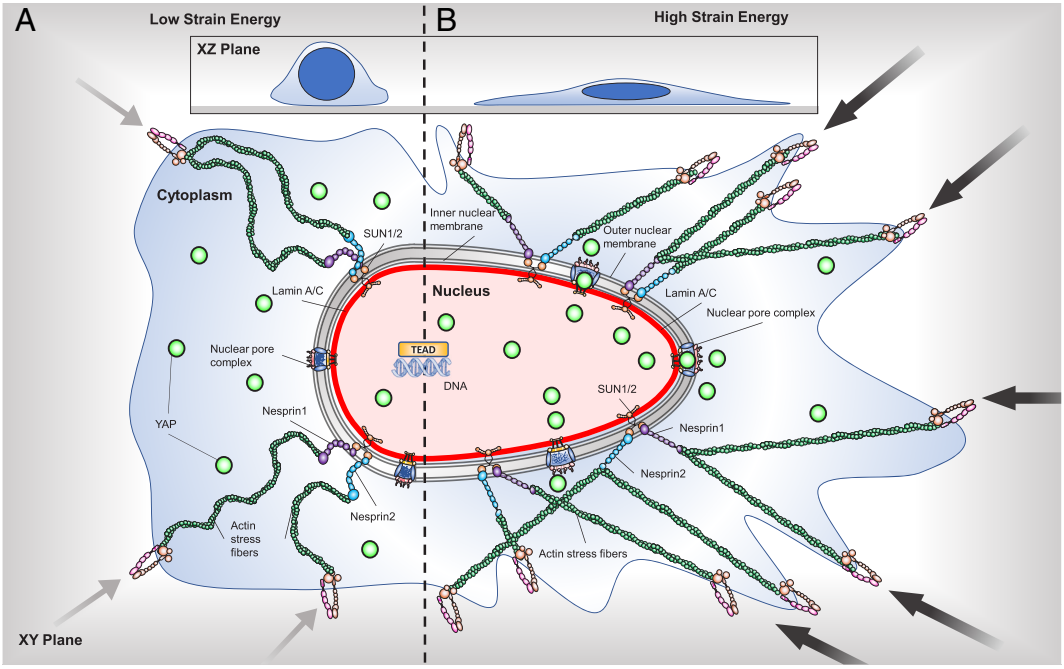

Fig. 6. Schematic of the proposed model for YAP nuclear translocation driven by nuclear compression arising from contractile work: (*A*) Cell exerting low contractile work (low strain energy) is representative of a low-tensional state, exhibiting loose actin stress fibers, reduced contractile force transduction to the nucleus via LINC complex, resulting in uncompressed nuclei (XZ plane) and lower YAP nuclear localization. (*B*) Cell exerting high contractile work (high strain energy) is representative of a high-tensional state, exhibiting tensed actin stress fibers, high contractile force transduction to the nucleus via LINC complex, resulting in compressed nuclei (XZ plane) with stretched nuclear pore complex, and increased YAP nuclear localization.

then identified that total cell contractile work is a better predictor of YAP activity than cell traction stress all substrates. We showed that this contractile work compresses the nucleus and that while the LINC complex is not required for YAP mechanotransduction, it increases the efficiency of mechanical coupling and actomyosin contractile deformation of the nucleus (*SI Appendix*, Fig. S4).

We also investigated the role of nuclear compliance on the amount of the cell contractile work (strain energy) required to trigger YAP nuclear translocation. We observed that nuclear stiffness scales with lamA/C expression levels in agreement with previous findings (35, 61). For a given amount of contractile work, softer nuclei were compressed more than stiffer nuclei and displayed higher YAP localization, revealing that contractility does not proscribe YAP activity. Regardless of nuclear stiffness, contractility, or microenvironment stiffness, all nuclei exhibited the same trend of YAP localization with respect to nuclear volume. This relationship held true even in unphysiological cells with depolymerized actin or under external osmotic stress. Regulation via nuclear compression offers a mechanistic explanation for previous observations that YAP activity is increased in lamin deficient cells (72, 73) and suggests that softer nuclei may be expected to have increased YAP localization. This is consistent with previous reports suggesting that nuclear softening, which often occurs in malignant cancer cells (74, 75), would promote YAP nuclear entry (30, 76). It is also consistent with previous studies of lamA reduction (59, 60) and increased YAP activity in cancer progression (15, 36, 74, 75, 77). In the context of cell differentiation, our proposed mechanism of nuclear-compression YAP regulation agrees with previous reports of cell compression (63, 78) and elevated cell contractility (5, 79, 80) mediating osteogenic differentiation as a result of YAP activation.

We anticipate that this link between cell strain energy, nuclear stiffness, nuclear compression, and YAP activity will offer insight and potential therapeutic strategies for other diverse diseases associated with modified nuclear mechanics and cellular dysfunction, including aging disorders (81), Emery–Dreifuss muscular dystrophy (40), and Hutchinson–Gilford progeria syndrome (41); aclearer understanding of mechanical YAP regulation will also provide better strategies for directing stem cell engineering.

Materials and Methods

Fabrication of PDMS Substrates. To determine the effects of substrate rigidity on dynamic localization of EGFP-YAP protein, PDMS substrates with different stiffnesses were prepared as described previously (51, 52).

PAA Fabrication. PAA gels were prepared based on the previously described protocol (82).

Transfection and Confocal Microscopy of Live Cells. To quantitatively track EGFP-YAP mechanotransduction with time**,** we transiently transfected NIH-3T3 cells with two plasmids, pEGFP-yap-C3-hYAP1 (Addgene, plasmid #17843) (17) and EBFP2-Nucleus-7 (nuclear localization signal, Addgene, plasmid #55249), using GenJet transfection reagent (SignaGen). Eighteen to twenty-four hours later, cells were seeded on fibronectin-coated PDMS, PAA, and glass substrates, and after cell attachment, they were transferred to a lab-built heated stage perfused with 5% CO_2 and mounted on a confocal microscope (Leica TCS SP8 with a 10× 0.4NA objective).

In order to examine the effects of the LINC complex on contractile and force-mediated nuclear compression and YAP translocation, we transfected the cells with two dominant-negative GFP-Nesprin1-KASH and GFP-Nesprin2-KASH (DNK1/2) plasmids which were kindly provided by Dr. Catherin Shanahan's laboratory (King's College, London) (30, 83).

TFM. Traction forces are those applied by the cells to their underlying substrates during adhesion, spreading, and migration. Active contractile stress in the actin cytoskeleton was quantified using TFM as previously described (52, 56).

Cell-substrate traction stresses and strain energies were calculated for each acquired time frame as described previously (56).

Quantification and Modulating of LamA/C Expression. To quantify the total lamA/C present in the nuclei, all the cells were transfected with GFP-tagged lamA/C Chromobody (Chromtek) which facilitates real-time imaging of lamA/C by labeling the total lamA/C without interfering with its function and distribution in the nuclei (61, 62).

Volume Measurement of Nuclei. In order to measure nuclear volume and nuclear compression, XYZ stacks of EBFP tagged nuclei with a z-step size of 0.5 μm were imaged using a Leica SP8 confocal microscope with 63×/1.4NA oil immersion objective lens and a pinhole of 1 AU, resulting in an axial Full Width Half Maximum optical thickness of 0.5 μm. The 3D visualization and quantification were performed with Fiji software. To quantify nuclear volume, the stacks were thresholded based on the top and bottom of the nuclei, and then, the number of voxels of the thresholded region was counted and multiplied by the size of each voxel using Fiji software. Cell cycles were not synchronized, potentially contributing to the observed variation and larger nuclear volumes. To investigate the role of cell contractility in nuclear compression and YAP localization in WT and lamA/C siRNA cells, we employed z stacks imaging of the EBFP tagged nuclei of the single cells seeded on PDMS substrates coated with fluorescent particles at the same time when near infrared fluorescent protein conjugated (iRFP)-YAP, EBFP-Nucleus, GFP-Chromobody, and fluorescent particles were imaged. To analyze traction stresses and strain energies of the cells, at the end of the experiment, cells were detached for the null force image. We repeated the same experiment for LINC disrupted cells and CytoD treated cells to investigate how LINC complex disruption and actin filament depolymerization affect contractile force–mediated nuclear compression.

Osmotic Compression. To examine how external nuclear compression regulates YAP localization, hyperosmotic pressure was applied using different concentrations of 400 Da PEG (PEG 400, Sigma) (61, 63, 84).

Quantification of Nuclear Bulk Moduli. To determine how nuclear stiffness influenced the required force to activate YAP, we modulated the lamA/C expression level as described above. Eighteen hours after seeding the cells on fibronectin-coated glasses, we applied different hyperosmotic pressures using different concentrations of PEG400 as mentioned above. We acquired XYZ stacks of EBFP-Nucleus before and after adding PEG. We then quantified change in the nuclear volume when the cells with different lamA/C expression levels were exposed to different hyperosmotic shocks, and using $B = -\Delta P/(\Delta V/V_0)$, where B = bulk modulus, ΔP = osmotic pressure, ΔV = change in nuclear volume, and V_0 = Initial nuclear volume, we calculated nuclear bulk modulus (61, 84).

Data, Materials, and Software Availability. All calculations and analysis were performed using MATLAB, Python, and ImageJ. Scripts are available from Github (https://github.com/NewshaKoushki/pnas2023_paper_tools) (85).

ACKNOWLEDGMENTS. We sincerely thank Xavier Trepat and Shanahan Catherine for the kind gifts of plasmids (iRFP-YAP, dominant-negative EGFP-Nesprin1-KASH and EGFP-Nesprin2-KASH), Qiuping Zhang, Rosa Kaviani, and Johanan Idicula for helpful discussions, and Chris Sitaras for helping in plasmid sequencing. We thank Katherine Ehrlicher and Philippe Bergeron for their assistance in copyediting the manuscript. We acknowledge support from grants Natural Sciences and Engineering Research Council of Canada (NSERC) RGPIN/05843-2014 and NSERC EQPEQ/472339-2015, Canadian Institutes of Health Research Grant #143327, and Canadian Foundation for Innovation Projects #32749 and #39725.

1. V. Vogel, M. Sheetz, Local force and geometry sensing regulate cell functions. *Nat. Rev. Mol. Cell Biol.* **7**, 265–275 (2006), 10.1038/nrm1890.
2. C. Hahn, M. A. Schwartz, The role of cellular adaptation to mechanical forces in atherosclerosis. *Arterioscler Thromb. Vasc. Biol.* **28**, 2101–2107 (2008), 10.1161/atvbaha.108.165951.
3. S. Cho, J. Irianto, D. E. Discher, Mechanosensing by the nucleus: From pathways to scaling relationships. *J. Cell Biol.* **216**, 305–315 (2017), 10.1083/jcb.201610042.
4. T. P. Driscoll, B. D. Cosgrove, S. J. Heo, Z. E. Shurden, R. L. Mauck, Cytoskeletal to nuclear strain transfer regulates YAP signaling in mesenchymal stem cells. *Biophys. J.* **108**, 2783–2793 (2015), 10.1016/j.bpj.2015.05.010.
5. S. Dupont *et al.*, Role of YAP/TAZ in mechanotransduction. *Nature* **474**, 179–183 (2011), 10.1038/nature10137.
6. J. D. Humphrey, E. R. Dufresne, M. A. Schwartz, Mechanotransduction and extracellular matrix homeostasis. *Nat. Rev. Mol. Cell Biol.* **15**, 802–812 (2014), 10.1038/nrm3896.
7. M. Pavel *et al.*, Contact inhibition controls cell survival and proliferation via YAP/TAZ-autophagy axis. *Nat. Commun.* **9**, 2961 (2018), 10.1038/s41467-018-05388-x.
8. S. Piccolo, S. Dupont, M. Cordenonsi, The biology of YAP/TAZ: Hippo signaling and beyond. *Physiol. Rev.* **94**, 1287–1312 (2014), 10.1152/physrev.00005.2014.
9. B. Zhao, L. Li, Q. Lei, K. L. Guan, The Hippo-YAP pathway in organ size control and tumorigenesis: An updated version. *Genes Dev.* **24**, 862–874 (2010), 10.1101/gad.1909210.
10. N. Koushki *et al.*, A new injectable biphasic hydrogel based on partially hydrolyzed polyacrylamide and nanohydroxyapatite as scaffold for osteochondral regeneration. *RSC Adv.* **5**, 9089–9096 (2015), 10.1039/C4RA10890F.
11. O. Dobrokhotov, M. Samsonov, M. Sokabe, H. Hirata, Mechanoregulation and pathology of YAP/TAZ via Hippo and non-Hippo mechanisms. *Clin. Transl. Med.* **7**, 23–23 (2018), 10.1186/s40169-018-0202-9.
12. I. Lian *et al.*, The role of YAP transcription coactivator in regulating stem cell self-renewal and differentiation. *Genes Dev.* **24**, 1106–1118 (2010), 10.1101/gad.1903310.
13. E. Donato *et al.*, YAP and TAZ are dispensable for physiological and malignant haematopoiesis. *Leukemia* **32**, 2037–2040 (2018), 10.1038/s41375-018-0111-3.
14. X. Varelas, The Hippo pathway effectors TAZ and YAP in development, homeostasis and disease. *Development* **141**, 1614–1626 (2014), 10.1242/dev.102376.
15. F. Zanconato, M. Cordenonsi, S. Piccolo, YAP/TAZ at the roots of cancer. *Cancer Cell* **29**, 783–803 (2016), 10.1016/j.ccell.2016.05.005.
16. J. Y. Lee *et al.*, YAP-independent mechanotransduction drives breast cancer progression. *Nat. Commun.* **10**, 1848 (2019), 10.1038/s41467-019-09755-0.
17. S. Basu, N. F. Totty, M. S. Irwin, M. Sudol, J. Downward, Akt phosphorylates the Yes-associated protein, YAP, to induce interaction with 14–3-3 and attenuation of p73-mediated apoptosis. *Mol. Cell* **11**, 11–23 (2003), 10.1016/s1097-2765(02)00776-1.
18. M. P. Scheid, J. R. Woodgett, PKB/AKT: Functional insights from genetic models. *Nat. Rev. Mol. Cell Biol.* **2**, 760–768 (2001), 10.1038/35096067.
19. H. Xie, L. Wu, Z. Deng, Y. Huo, Y. Cheng, Emerging roles of YAP/TAZ in lung physiology and diseases. *Life Sci.* **214**, 176–183 (2018), 10.1016/j.lfs.2018.10.062.
20. A. Das, R. S. Fischer, D. Pan, C. M. Waterman, YAP nuclear localization in the absence of cell-cell contact is mediated by a filamentous actin-dependent, Myosin II- and phospho-YAP-independent pathway during extracellular matrix mechanosensing. *J. Biol. Chem.* **291**, 6096–6110 (2016), 10.1074/jbc.M115.708313.
21. A. Elosegui-Artola *et al.*, Mechanical regulation of a molecular clutch defines force transmission and transduction in response to matrix rigidity. *Nat. Cell Biol.* **18**, 540–548 (2016), 10.1038/ncb3336.
22. N. Huebsch *et al.*, Harnessing traction-mediated manipulation of the cell/matrix interface to control stem-cell fate. *Nat. Mater.* **9**, 518–526 (2010), 10.1038/nmat2732.
23. J. Oliver-De La Cruz *et al.*, Substrate mechanics controls adipogenesis through YAP phosphorylation by dictating cell spreading. *Biomaterials* **205**, 64–80 (2019), 10.1016/j.biomaterials.2019.03.009.
24. A. Totaro, T. Panciera, S. Piccolo, YAP/TAZ upstream signals and downstream responses. *Nat. Cell Biol.* **20**, 888–899 (2018), 10.1038/s41556-018-0142-z.
25. M. Fischer, P. Rikeit, P. Knaus, C. Coirault, YAP-mediated mechanotransduction in skeletal muscle. *Front. Physiol.* **7**, 41 (2016), 10.3389/fphys.2016.00041.
26. L. Valon, A. Marín-Llauradó, T. Wyatt, G. Charras, X. Trepat, Optogenetic control of cellular forces and mechanotransduction. *Nat. Commun.* **8**, 14396 (2017), 10.1038/ncomms14396.
27. M. A. Wozniak, C. S. Chen, Mechanotransduction in development: A growing role for contractility. *Nat. Rev. Mol. Cell Biol.* **10**, 34–43 (2009), 10.1038/nrm2592.
28. A. J. Ehrlicher, F. Nakamura, J. H. Hartwig, D. A. Weitz, T. P. Stossel, Mechanical strain in actin networks regulates FilGAP and integrin binding to filamin A. *Nature* **478**, 260–263 (2011), 10.1038/nature10430.
29. F. Alisafaei, D. S. Jokhun, G. V. Shivashankar, V. B. Shenoy, Regulation of nuclear architecture, mechanics, and nucleocytoplasmic shuttling of epigenetic factors by cell geometric constraints. *Proc. Natl. Acad. Sci. U.S.A.* **116**, 13200–13209 (2019), 10.1073/pnas.1902035116.
30. A. Elosegui-Artola *et al.*, Force triggers YAP nuclear entry by regulating transport across nuclear pores. *Cell* **171**, 1397–1410.e1314 (2017), 10.1016/j.cell.2017.10.008.
31. M. Maurer, J. Lammerding, The driving force: Nuclear mechanotransduction in cellular function, fate, and disease. *Annu. Rev. Biomed. Eng.* **21**, 443–468 (2019), 10.1146/annurev-bioeng-060418-052139.
32. S. E. Szczesny, R. L. Mauck, The nuclear option: Evidence implicating the cell nucleus in mechanotransduction. *J. Biomech. Eng.* **139**, 0210061–02100616 (2017), 10.1115/1.4035350.
33. A. Athirasala, N. Hirsch, A. Buxboim, Nuclear mechanotransduction: Sensing the force from within. *Curr. Opin. Cell Biol.* **46**, 119–127 (2017), 10.1016/j.ceb.2017.04.004.
34. J. Lammerding, Mechanics of the nucleus. *Compr. Physiol.* **1**, 783–807 (2011), 10.1002/cphy.c100038.
35. J. Lammerding *et al.*, Lamins A and C but not lamin B1 regulate nuclear mechanics. *J. Biol. Chem.* **281**, 25768–25780 (2006), 10.1074/jbc.M513511200.
36. J. Lammerding *et al.*, Lamin A/C deficiency causes defective nuclear mechanics and mechanotransduction. *J. Clin. Invest.* **113**, 370–378 (2004), 10.1172/JCI19670.
37. C. Guilluy *et al.*, Isolated nuclei adapt to force and reveal a mechanotransduction pathway in the nucleus. *Nat. Cell Biol.* **16**, 376–381 (2014), 10.1038/ncb2927.
38. L. Hanson *et al.*, Vertical nanopillars for in situ probing of nuclear mechanics in adherent cells. *Nat. Nanotechnol.* **10**, 554–562 (2015), 10.1038/nnano.2015.88.
39. T. Harada *et al.*, Nuclear lamin stiffness is a barrier to 3D migration, but softness can limit survival. *J. Cell Biol.* **204**, 669–682 (2014), 10.1083/jcb.201308029.
40. G. Bonne *et al.*, Mutations in the gene encoding lamin A/C cause autosomal dominant Emery-Dreifuss muscular dystrophy. *Nat. Genet.* **21**, 285–288 (1999), 10.1038/6799.
41. A. De Sandre-Giovannoli *et al.*, Lamin a truncation in Hutchinson-Gilford progeria. *Science (New York, N.Y.)* **300**, 2055 (2003), 10.1126/science.1084125.
42. C. Capo-Chichi *et al.*, Loss of A-type lamin expression compromises nuclear envelope integrity in breast cancer. *Chinese J. Cancer* **30**, 415–425 (2011), 10.5732/cjc.010.10566.
43. C. Denais, J. Lammerding, Nuclear mechanics in cancer. *Adv. Exp. Med. Biol.* **773**, 435–470 (2014), 10.1007/978-1-4899-8032-8 _ 20.
44. J. Irianto, C. R. Pfeifer, I. L. Ivanovska, J. Swift, D. E. Discher, Nuclear lamins in cancer. *Cell Mol. Bioeng.* **9**, 258–267 (2016), 10.1007/s12195-016-0437-8.
45. Y. Cui *et al.*, Cyclic stretching of soft substrates induces spreading and growth. *Nat. Commun.* **6**, 6333 (2015), 10.1038/ncomms7333.
46. J. M. Franklin, R. P. Ghosh, Q. Shi, M. P. Reddick, J. T. Liphardt, Concerted localization-resets precede YAP-dependent transcription. *Nat. Commun.* **11**, 4581 (2020), 10.1038/s41467-020-18368-x.
47. J. P. Califano, C. A. Reinhart-King, Substrate stiffness and cell area predict cellular traction stresses in single cells and cells in contact. *Cell Mol. Bioeng.* **3**, 68–75 (2010), 10.1007/s12195-010-0102-6.
48. C. M. Lo, H. B. Wang, M. Dembo, Y. L. Wang, Cell movement is guided by the rigidity of the substrate. *Biophys. J.* **79**, 144–152 (2000), 10.1016/S0006-3495(00)76279-5.
49. A. Mertz *et al.*, Scaling of traction forces with the size of cohesive cell colonies. *Phys. Rev. Lett.* **108**, 198101 (2012), 10.1103/PhysRevLett.108.198101.

50. K. E. Scott, S. I. Fraley, P. Rangamani, A spatial model of YAP/TAZ signaling reveals how stiffness, dimensionality, and shape contribute to emergent outcomes. *Proc. Natl. Acad. Sci. U.S.A.* **118**, e2021571118 (2021), 10.1073/pnas.2021571118.
51. H. Yoshie *et al.*, High throughput traction force microscopy using pdms reveals dose-dependent effects of transforming growth factor-β on the epithelial-to-mesenchymal transition. *JoVE* **148**, e59364 (2019), 10.3791/59364.
52. H. Yoshie *et al.*, Traction force screening enabled by compliant PDMS elastomers. *Biophys. J.* **114**, 2194–2199 (2018), 10.1016/j.bpj.2018.02.045.
53. B. Trappmann *et al.*, Extracellular-matrix tethering regulates stem-cell fate. *Nat. Mater.* **11**, 642–649 (2012).
54. J. H. Wen *et al.*, Interplay of matrix stiffness and protein tethering in stem cell differentiation. *Nat. Mater.* **13**, 979–987 (2014), 10.1038/nmat4051.
55. J.-Y. Shiu, L. Aires, Z. Lin, V. Vogel, Nanopillar force measurements reveal actin-cap-mediated YAP mechanotransduction. *Nat. Cell Biol.* **20**, 262–271 (2018), 10.1038/s41556-017-0030-y.
56. J. P. Butler, I. M. Tolic-Norrelykke, B. Fabry, J. J. Fredberg, Traction fields, moments, and strain energy that cells exert on their surroundings. *Am. J. Physiol. Cell Physiol.* **282**, C595–605 (2002), 10.1152/ajpcell.00270.2001.
57. P. W. Oakes, S. Banerjee, M. C. Marchetti, M. L. Gardel, Geometry regulates traction stresses in adherent cells. *Biophys. J.* **107**, 825–833 (2014), 10.1016/j.bpj.2014.06.045.
58. T. J. Kirby, J. Lammerding, Emerging views of the nucleus as a cellular mechanosensor. *Nat. Cell Biol.* **20**, 373–381 (2018), 10.1038/s41556-018-0038-y.
59. A. Buxboim *et al.*, Matrix elasticity regulates lamin-A, C phosphorylation and turnover with feedback to actomyosin. *Curr. Biol.* **24**, 1909–1917 (2014), 10.1016/j.cub.2014.07.001.
60. J. Swift *et al.*, Nuclear lamin-A scales with tissue stiffness and enhances matrix-directed differentiation. *Science* **341**, 1240104 (2013), 10.1126/science.1240104.
61. L. K. Srivastava, Z. Ju, A. Ghagre, A. J. Ehrlicher, Spatial distribution of lamin A/C determines nuclear stiffness and stress-mediated deformation. *J. Cell Sci.* **134**, jcs248559 (2021), 10.1242/jcs.248559.
62. K. Zolghadr, J. Gregor, H. Leonhardt, U. Rothbauer, Case study on live cell apoptosis-assay using lamin-chromobody cell-lines for high-content analysis. *Methods Mol. Biol.* **911**, 569–575 (2012), 10.1007/978-1-61779-968-6 _ 36.
63. M. Guo *et al.*, Cell volume change through water efflux impacts cell stiffness and stem cell fate. *Proc. Natl. Acad. Sci. U.S.A.* **114**, E8618–e8627 (2017), 10.1073/pnas.1705179114.
64. A. D. Stephens, E. J. Banigan, S. A. Adam, R. D. Goldman, J. F. Marko, Chromatin and lamin A determine two different mechanical response regimes of the cell nucleus. *Mol. Biol. Cell* **28**, 1984–1996 (2017), 10.1091/mbc.e16-09-0653.
65. E. Hockly *et al.*, Suberoylanilide hydroxamic acid, a histone deacetylase inhibitor, ameliorates motor deficits in a mouse model of Huntington's disease. *Proc. Natl. Acad. Sci. U.S.A.* **100**, 2041–2046 (2003), 10.1073/pnas.0437870100.
66. P. A. Marks, R. Breslow, Dimethyl sulfoxide to vorinostat: Development of this histone deacetylase inhibitor as an anticancer drug. *Nat. Biotechnol.* **25**, 84–90 (2007), 10.1038/nbt1272.
67. M. Aragona *et al.*, A mechanical checkpoint controls multicellular growth through YAP/TAZ regulation by actin-processing factors. *Cell* **154**, 1047–1059 (2013), 10.1016/j.cell.2013.07.042.
68. T. P. Driscoll, B. D. Cosgrove, S.-J. Heo, Z. E. Shurden, R. L. Mauck, Cytoskeletal to nuclear strain transfer regulates YAP signaling in mesenchymal stem cells. *Biophys. J.* **108**, 2783–2793 (2015), 10.1016/j.bpj.2015.05.010.
69. Z. Cheng *et al.*, The surface stress of biomedical silicones is a stimulant of cellular response. *Sci. Adv.* **6**, eaay0076 (2020), 10.1126/sciadv.aay0076.
70. B. Trappmann *et al.*, Extracellular-matrix tethering regulates stem-cell fate. *Nat. Mater.* **11**, 642–649 (2012), 10.1038/nmat3339.
71. S. A. Manning *et al.*, Dynamic fluctuations in subcellular localization of the hippo pathway effector yorkie in vivo. *Curr. Biol.* **28**, 1651–1660.e1654 (2018), 10.1016/j.cub.2018.04.018.
72. D. J. Owens *et al.*, Lamin mutations cause increased YAP nuclear entry in muscle stem cells. *Cells* **9**, 816 (2020), 10.3390/cells9040816.
73. O. N. Wiggan, J. G. DeLuca, T. J. Stasevich, J. R. Bamburg, Lamin A/C deficiency enables increased myosin-II bipolar filament ensembles that promote divergent actomyosin network anomalies through self-organization. *Mol. Biol. Cell* **31**, 2363–2378 (2020), 10.1091/mbc.E20-01-0017-T.
74. S. E. Cross, Y.-S. Jin, J. Rao, J. K. Gimzewski, Nanomechanical analysis of cells from cancer patients. *Nat. Nanotechnol.* **2**, 780–783 (2007), 10.1038/nnano.2007.388.
75. J. Guck *et al.*, Optical deformability as an inherent cell marker for testing malignant transformation and metastatic competence. *Biophys. J.* **88**, 3689–3698 (2005), 10.1529/biophysj.104.045476.
76. T. Shimomura *et al.*, The PDZ-binding motif of Yes-associated protein is required for its co-activation of TEAD-mediated CTGF transcription and oncogenic cell transforming activity. *Biochem. Biophys. Res. Commun.* **443**, 917–923 (2014), 10.1016/j.bbrc.2013.12.100.
77. I. M. Alhudiri *et al.*, Expression of Lamin A/C in early-stage breast cancer and its prognostic value. *Breast Cancer Res. Treatment* **174**, 661–668 (2019), 10.1007/s10549-018-05092-w.
78. M. Bao *et al.*, Cellular volume and matrix stiffness direct stem cell behavior in a 3D microniche. *ACS Appl. Mater. Interfaces* **11**, 1754–1759 (2019), 10.1021/acsami.8b19396.
79. B. C. Heng *et al.*, Role of YAP/TAZ in cell lineage fate determination and related signaling pathways. *Front. Cell Dev. Biol.* **8**, 735–735 (2020), 10.3389/fcell.2020.00735.
80. X. Xue, X. Hong, Z. Li, C. X. Deng, J. Fu, Acoustic tweezing cytometry enhances osteogenesis of human mesenchymal stem cells through cytoskeletal contractility and YAP activation. *Biomaterials* **134**, 22–30 (2017), 10.1016/j.biomaterials.2017.04.03.
81. V. Verstraeten, J. Ji, K. Cummings, R. Lee, J. Lammerding, Increased mechanosensitivity and nuclear stiffness in Hutchinson-Gilford progeria cells: Effects of farnesyltransferase inhibitors. *Aging cell* **7**, 383–393 (2008), 10.1111/j.1474-9726.2008.00382.x.
82. T. Yeung *et al.*, Effects of substrate stiffness on cell morphology, cytoskeletal structure, and adhesion. *Cell Motil Cytoskeleton* **60**, 24–34 (2005), 10.1002/cm.20041.
83. M. L. Lombardi *et al.*, The interaction between nesprins and sun proteins at the nuclear envelope is critical for force transmission between the nucleus and cytoskeleton. *J. Biol. Chem.* **286**, 26743–26753 (2011). 10.1074/jbc.M111.233700.
84. A. Khavari, A. J. Ehrlicher, Nuclei deformation reveals pressure distributions in 3D cell clusters. *PloS One* **14**, e0221753 (2019), 10.1371/journal.pone.0221753.
85. N. Koushki, PNAS 2023 analysis scripts. Github. https://github.com/NewshaKoushki/pnas2023_paper_tools. Deposited 7 May 2023.